Hidden-order symmetry and superconductivity in URu_2Si_2 investigated by quasiparticle interference

Alireza Akbari[1,2] and Peter Thalmeier[3]
[1]*Max Planck Institute for Solid State Research, D-70569 Stuttgart, Germany*
[2]*Asia Pacific Center for Theoretical Physics, POSTECH, Pohang, Gyeongbuk 790-784, Korea*
[3]*Max Planck Institute for the Chemical Physics of Solids, D-01187 Dresden, Germany*
(Received 9 October 2014; revised manuscript received 2 December 2014; published 15 December 2014)

The hidden order (HO) in URu_2Si_2 has been determined as a high-rank multipole formed by itinerant $5f$ electrons with distinct orbital structure imposed by the crystalline electric field. Because this can lead to a considerable number of different multipoles, it is of great importance to use microscopic techniques that are sensitive to their subtle physical differences. Here, we investigate whether the quasiparticle interference (QPI) method can distinguish between the two most frequently proposed HO parameter models: the even rank-4 hexadecapole and the odd-rank-5 dotriacontapole model. We obtain the quasiparticle dispersion and reconstructed Fermi surface in each HO phase adapting an effective two-orbital model of $5f$ bands that reproduces the main Fermi surface sheets of the para phase. We show that the resulting QPI spectrum reflects directly the effect of fourfold symmetry breaking in the rank-5 model, which is absent in the rank-4 model. Therefore we suggest that the QPI method should give the possibility of a direct discrimination between the two most investigated models of HO in URu_2Si_2. Furthermore, the signature of proposed chiral d-wave superconducting (SC) order parameter in QPI of the coexisting HO + SC phase is investigated.

DOI: 10.1103/PhysRevB.90.224511 PACS number(s): 74.20.Rp, 74.55.+v, 75.30.Mb

I. INTRODUCTION

The nature of hidden order (HO) in URu_2Si_2 is considered a central topic in the investigation of strongly correlated electron systems [1]. For its theoretical analysis several fundamental issues arise. Initially, the HO was described in terms of tetragonal crystalline electric field (CEF) split localized $5f^2$ (U^{4+}) states [2]. Their localized multipoles would then experience effective RKKY-type intersite interactions leading to their long-range order below $T_{HO} = 17.5$ K. In fact, the thermodynamic properties of the HO transition may be described within the localized context [2].

However, later ARPES experiments [3] and theoretical analysis [4] suggested that the $5f$ electrons have itinerant character and their Fermi surface (FS) reconstruction below T_{HO} plays an essential role in the HO mechanism. The hidden order parameter then should be constructed from itinerant $5f$ basis states rather than localized ones. This was carried out by Ikeda *et al.* [5] within an extended many-body model starting from band structure calculations. It was found that the antiferro-type HO evolves due to a nesting between Γ- and Z-centered electron and hole pockets with a wave vector $\mathbf{Q} = (0,0,1)$. Because they are mainly formed by orbitals with a large total angular momentum ($j = \frac{5}{2}$) component, $M = \pm\frac{3}{2}, \pm\frac{5}{2}$, the dominating AF hidden order parameter is a multipole of rank-5 (E_-) type, which breaks translational, c-axis C_4 rotational, and time-reversal symmetries. As an alternative possibility, we also include the rank-4 (A_{2+}) hexadecapole order [2,6] in our treatment, which breaks translational and diagonal in-plane reflection symmetries but preserves C_4 rotations and time reversal. The evolution of hidden order leads to a characteristic reconstruction of the Fermi surface: due to doubling of the unit cell, the Z-point hole pocket is downfolded to the Γ point of the Brillouin zone (BZ) and electron and hole pockets are broken into the smaller FS sheets at their crossing points. Concurrently a HO gap evolves in the density of states (DOS).

Deep inside the HO phase, unconventional heavy fermion superconductivity appears at $T_c = 1.45$ K, which was suggested to have chiral d-wave symmetry [7], but this, so far, remains a conjecture. It coexists homogeneously with HO and vanishes at the same critical pressure $p_c \simeq 0.75$ kbar. Recently, the quasiparticle interference (QPI) method has been proven very successful in unraveling the gap symmetry of heavy fermion superconductors [8–10]. Already before [11] the method was demonstrated in the HO phase of URu_2Si_2 but not yet in the coexistence region with superconductivity (SC + HO).

Here, we present a theoretical analysis of QPI both in the HO state and coexisting HO + SC phase. Our main goal is to understand the principal effects that the FS reconstruction due to HO has on the QPI and whether this holds any clue to the symmetry of the HO phase. For that purpose, we make a comparative analysis of reconstructed bands and Fermi surfaces as well as QPI spectra for the most frequently involved HO symmetries, namely, the doubly degenerate rank-5 E_- dotriacontapole [5] and the nondegenerate antiferro-type rank-4 hexadecapole [2,6] introduced above.

For this purpose, we start from an effective $5f$ electron band model describing the Γ and Z-point electron and hole pockets (but not the small pockets on the A and M points of folded BZ corners), which was introduced by Rau and Kee [12]. We give closed expressions for the reconstructed quasiparticle bands in the HO phase for both models in the whole BZ. Using this result, we can calculate with high accuracy the expected QPI spectrum, map its characteristic structures and relate them to the reconstructed HO Fermi surface. We also discuss possible connections to the experimental results [11]. Finally, we include a BCS term for the reconstructed HO bands with a SC gap symmetry of the chiral d-wave type. This allows us to predict the QPI spectrum in the coexisting HO + SC phase, which has not yet been performed experimentally. We will finally discuss the features in QPI that

may be taken as typical consequence of the chiral d-wave symmetry.

II. TWO-ORBITAL MODEL OF HEAVY ELECTRON BANDS IN URu_2Si_2

In this work, we are interested in the very low energy ($\simeq$1 meV) quasiparticle spectroscopy of URu_2Si_2, therefore it is reasonable to start with an effective low-energy model of the heavy electron bands. It should be simple enough to enable analytical representation of the dispersion and high-resolution computation of the QPI spectrum. But it must also have enough complexity to allow for modeling of realistic Fermi surface features, in particular, the electron hole nesting property at wave vector $\mathbf{Q} = (2\pi/c)\hat{\mathbf{z}} = (0,0,1)$ in r.l.u. (reduced lattice units) because the latter leads to the staggered hidden order parameter. The kinetic energy may be constructed from hopping terms using the jj-coupled single electron $5f$ states (j = total angular momentum) with incorporated spin-orbit (s.o.) coupling and orbital symmetries that are adapted to the local tetragonal crystalline electric field (CEF) potential at U sites. Such a procedure has been used successfully before in Refs. [5,13–15]. Since the s.o. splitting of U is very large, the $j = 7/2$ orbitals are neglected, taking only the $j = 5/2$ states, which are CEF split into three Kramers doublets $\Gamma_7^{(\alpha)}$ ($\alpha = 1,2$) and Γ_6. For the formation of high-order multipoles discussed here, a further restriction to the two $\Gamma_7^{(\alpha)}$ doublets is possible. This is also suggested by *ab initio* calculations of electron and hole pockets close to the Fermi surface [4,5]. These basis states are then created by $f^\dagger_{\alpha\sigma}$ where σ is the pseudospin ($\sigma = \pm$) of the doublets. They are related to the free ion states with total angular momentum component $j_z = M$ ($|M| \leqslant 5/2$) via the transformation

$$\begin{pmatrix} f_{1\pm} \\ f_{2\pm} \end{pmatrix} = \begin{pmatrix} \cos\theta & \sin\theta \\ -\sin\theta & \cos\theta \end{pmatrix} \begin{pmatrix} f_{\pm\frac{5}{2}} \\ f_{\mp\frac{3}{2}} \end{pmatrix}, \qquad (1)$$

where the mixing angle θ is determined by the tetragonal CEF parameters. A minimal kinetic energy model involving CEF splitting and effective hopping up to second nearest neighbors (see Appendix) was introduced by Rau and Kee (Ref. [12]) and is given by

$$H_0 = \sum_{\mathbf{k}\sigma} (A_{1\mathbf{k}} f^\dagger_{1\sigma\mathbf{k}} f_{1\sigma\mathbf{k}} + A_{2\mathbf{k}} f^\dagger_{2\sigma\mathbf{k}} f_{2\sigma\mathbf{k}}) + \sum_{\mathbf{k}} [D_{\mathbf{k}} (f^\dagger_{1+\mathbf{k}} f_{2-\mathbf{k}} - f^\dagger_{2+\mathbf{k}} f_{1-\mathbf{k}}) + \text{H.c.}], \qquad (2)$$

where the kinetic energy functions $A_{\alpha\mathbf{k}}$ and $D_{\mathbf{k}}$ are defined in Appendix. The above Hamiltonian directly parametrizes the heavy $5f$ quasiparticle states that form the electron and hole pockets. Therefore the hybridization with light electrons does not appear explicitly any more. In QPI spectroscopy, this constrains us to the low-energy region below the hybridization gap. The hybridization effects on local DOS were studied in Ref. [16]. The model band structure and Fermi surface with electron pocket around Γ point and hole pocket around Z (0,0,0.5) are shown in Fig. 1.

III. THE HIDDEN MULTIPOLAR ORDER PARAMETERS

The first step in the identification of spontaneous order, whether hidden or not, is the determination of broken symmetries. In URu_2Si_2, these are [15,17] (i) translational symmetry breaking due to the antiferro-HO wave vector $\mathbf{Q}$ (from band folding along k_z observed in ARPES [3,18]), (ii) broken C_4 rotational symmetry (from torque oscillations [19], cyclotron resonance splitting [20], and high-resolution x-ray diffraction [21]), and (iii) time reversal symmetry breaking (from NMR [22] and μSR [23] experiments). It was concluded in Refs. [5,15,17] that the rank-5 dotriacontapole is the most plausible candidate. However, frequently the rank-4 hexadecapole was also proposed [6,24] as a candidate, although it breaks only translational symmetry and reflectional in-plane symmetry but not time reversal. We will discuss both possibilities in this work.

First, we give a prescription how to construct the multipolar order parameters and their molecular fields from the f-electron basis operators. It was demonstrated [13,15] that all physical f-electron multipoles up to highest rank 5 can be expressed in

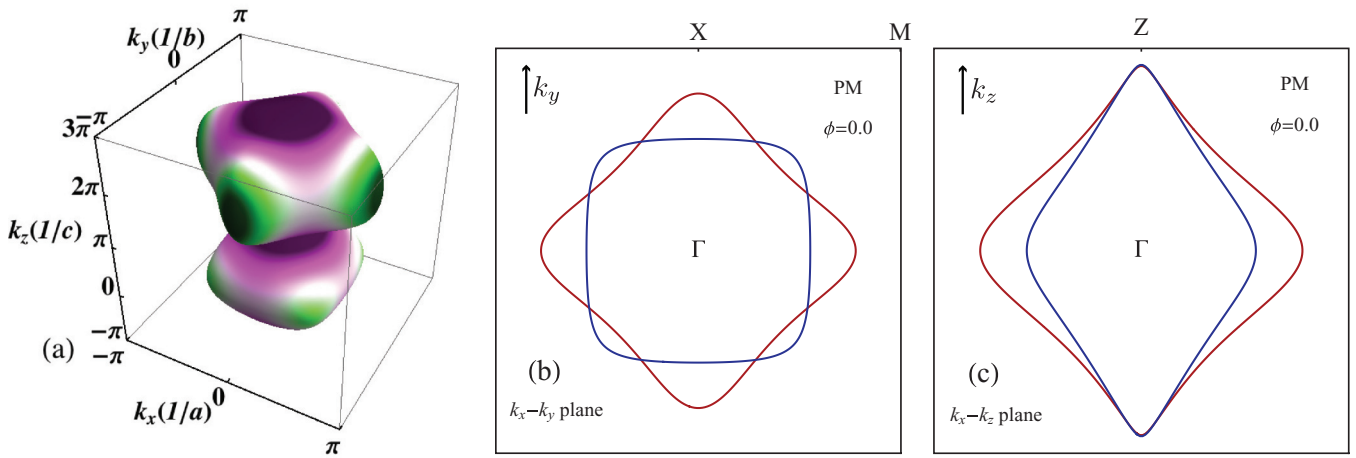

FIG. 1. (Color online) (a) Fermi surface sheets of URu_2Si_2 in the extended simple tetragonal (st) BZ with an electron sheet at Γ(0,0,0) and a hole sheet around $Z(0,0,2\pi/c)$ ($c \equiv 1$). The two sheets are nested by $\mathbf{Q} = (0,0,1)$. FS cuts with $k_z = 0$ (b) and $k_y = 0$ (c) in the reduced st BZ (Z-point folded onto Γ). The momentum range in (b) and (c) is given by $-\pi \leqslant k_i \leqslant \pi$.

terms of the charge operator

$$\rho_{\alpha\alpha'} = \frac{1}{2}\sum_{\sigma} f^{\dagger}_{\alpha\sigma} f_{\alpha'\sigma}, \tag{3}$$

and the pseudospin operator given by

$$S^{i}_{\alpha\alpha'} = \frac{1}{2}\sum_{\sigma\sigma'} f^{\dagger}_{\alpha\sigma}\sigma^{i}_{\sigma\sigma'} f_{\alpha'\sigma'}, \tag{4}$$

where generally $\alpha = 1,2,3$ denote the $\Gamma_7^{(1),(2)}$ and Γ_6 orbitals, respectively, and σ^i denotes a Pauli matrix with Cartesian index $i = x,y,z$. Since we restrict to the former, only multipoles with $\alpha,\alpha' = 1,2$ can be constructed. The two candidates discussed here belong to this class. The explicit forms of the one- and two-dimensional multipole representations at site i are given by

$$\text{hexadecapole, rank 4:}\quad \hat{\phi}_z^{A_{2+}}(i) = \frac{\mathrm{i}}{\sqrt{2}}\left(S^z_{12} - S^z_{21}\right)_i \tag{5}$$

and

$$\text{dotriacontapole, rank 5:}\quad \begin{cases} \hat{\phi}_x^{E_-}(i) = \frac{1}{\sqrt{2}}\left(S^x_{12} + S^x_{21}\right)_i \\ \hat{\phi}_y^{E_-}(i) = \frac{1}{\sqrt{2}}\left(S^y_{12} + S^y_{21}\right)_i \end{cases}. \tag{6}$$

To clarify the meaning of the multipoles, it is instructive to transform back to the free ion states using Eqs. (4) and (1). For simplicity, we choose the nondegenerate A_{2+} state. For the Fourier transform

$$\hat{\phi}_z^{A_{2+}}(\mathbf{q}) = \frac{1}{N}\sum_i \exp(\mathrm{i}\mathbf{q}\cdot\mathbf{R}_i)\hat{\phi}_z^{A_{2+}}(i),$$

we obtain

$$\begin{aligned}\hat{\phi}_z^{A_{2+}}(\mathbf{Q}) &= \hat{\phi}_z^{A_{2+}}(-\mathbf{Q})^{\dagger} \\ &= -\mathrm{i}\kappa\frac{1}{N}\sum_{\mathbf{k}}\sum_{|M|=\frac{3}{2},\frac{5}{2}} \sigma_M f^{\dagger}_{M-4\sigma_M;\mathbf{k}} f_{M;\mathbf{k}+\mathbf{Q}} \\ &= \mathrm{i}\kappa\frac{1}{N}\sum_{\mathbf{k}}\Big(f^{\dagger}_{\frac{5}{2}\mathbf{k}} f_{-\frac{3}{2}\mathbf{k}+\mathbf{Q}} + f^{\dagger}_{\frac{3}{2}\mathbf{k}} f_{-\frac{5}{2}\mathbf{k}+\mathbf{Q}} \\ &\quad - f^{\dagger}_{-\frac{5}{2}\mathbf{k}} f_{\frac{3}{2}\mathbf{k}+\mathbf{Q}} - f^{\dagger}_{-\frac{3}{2}\mathbf{k}} f_{\frac{5}{2}\mathbf{k}+\mathbf{Q}}\Big),\end{aligned} \tag{7}$$

where $\sigma_M = \mathrm{sign}(M) = \pm 1$ and $\kappa = 1/(2\sqrt{2}) = 0.35$. This explicit representation shows that the A_{2+} hexadecapole (rank 4) is formed by condensation of electron-hole pairs with momenta ($\mathbf{k}$, $\mathbf{k}$+$\mathbf{Q}$) in basis states that differ in angular momentum component by $\Delta M = \pm 4$, leading to the high multipole property. The common antiferromagnetic order (rank 1) would be formed by pairs that differ by $\Delta M = \pm 1$. Similarly, one may show that the E_- dotriakontapole (rank 5) is due to the condensation of pairs with a maximum angular momentum difference $\Delta M = \pm 5$. The effective interaction between f quasiparticles leads to the instability in these multipole channels [5]. The ordered phase is then described by an additional molecular field term in the Hamiltonian controlled by the multipole expectation values $\phi_n^{\Gamma}(\mathbf{Q}) = \langle\hat{\phi}_n^{\Gamma}(\mathbf{Q})\rangle$, where Γ denotes the representation and n is its degeneracy index. Using Eq. (4), these terms may be written as

$$\begin{aligned} A_{2+}: H_{\phi} &= -\mathrm{i}\kappa\phi_z^{\mathbf{Q}}\sum_{\mathbf{k}}(f^{\dagger}_{1\mathbf{k}}\sigma_z f_{2\mathbf{k}+\mathbf{Q}} - f^{\dagger}_{2\mathbf{k}}\sigma_z f_{1\mathbf{k}+\mathbf{Q}}) + \text{H.c.}, \\ E_-: H_{\phi} &= -\kappa\boldsymbol{\phi}^{\mathbf{Q}}\cdot\sum_{\mathbf{k}}(f^{\dagger}_{1\mathbf{k}}\boldsymbol{\sigma} f_{2\mathbf{k}+\mathbf{Q}} + f^{\dagger}_{2\mathbf{k}}\boldsymbol{\sigma} f_{1\mathbf{k}+\mathbf{Q}}) + \text{H.c.} \end{aligned} \tag{8}$$

Here, we introduced $f^{\dagger}_{\alpha\mathbf{k}} = (f^{\dagger}_{\alpha+\mathbf{k}}, f^{\dagger}_{\alpha-\mathbf{k}})$ with $\alpha = 1,2$ and $\sigma_z = \pm$ denoting band index and Kramers pseudospin, respectively. Furthermore, $\boldsymbol{\phi}^{\mathbf{Q}} = (\phi_x^{\mathbf{Q}}, \phi_y^{\mathbf{Q}})$ is the HO vector that expresses the twofold degeneracy of the E_- representation. Therefore right at T_{HO} the HO phase has continuous U(1) symmetry, which is lifted by higher order terms in the free energy below T_{HO}. Commonly, a phase with equal components $\phi_x^{\mathbf{Q}} = \phi_y^{\mathbf{Q}}$ called $E_-(1,1)$ phase or with only one nonzero $\phi_x^{\mathbf{Q}}$ or $\phi_y^{\mathbf{Q}}$ component called $E_-(1,0)$ or $E_-(0,1)$, respectively, is stabilized. In both cases, different domains are possible. For a discussion of the domain issue, we refer to Refs. [14,15]. A nonzero third component $\phi_z^{\mathbf{Q}}$ of the HO vector $\boldsymbol{\phi}$ [replacing $x,y \to z$ in Eq. (6)] would correspond to a different A_{2-} representation [5,12] that will not be considered here. We introduce the $2\otimes 4$ spinor basis $\Psi^{\dagger}_{\mathbf{k}} = (\psi^{\dagger}_{a\mathbf{k}}, \psi^{\dagger}_{b\mathbf{k}})$ with effective Kramers degenerate a,b components defined below for each HO symmetry separately. The total mean-field Hamiltonian, including the HO molecular fields may be written as

$$H = H_0 + H_{\phi} = \sum_{\mathbf{k}}\Psi^{\dagger}_{\mathbf{k}} h_{\mathbf{k}}\Psi_{\mathbf{k}};\quad h_{\mathbf{k}} = h_{a\mathbf{k}}\otimes h_{b\mathbf{k}}. \tag{9}$$

In the following, we will diagonalize this Hamiltonian consisting of two 4×4 blocks (a,b) explicitly in analytical form to calculate the reconstructed quasiparticle bands and the necessary Green's functions for QPI.

IV. QUASIPARTICLE EXCITATIONS IN THE HO PHASE

The HO molecular fields result in a splitting of Fermi surface states connected by a nesting vector. This will reconstruct the Fermi surface and equal energy surfaces close to the hot spots of the nesting. The details of the FS reconstruction should leave its imprint in the QPI spectrum. Since the reconstruction depends on the symmetries of HO, the QPI characteristics may allow to discriminate between them, in the same way as it does for different gap symmetries in an unconventional superconductor. For clarity, this analysis will be done separately for both HO candidates.

A. Dotriacontapole E_- phase

In this representation, it is most convenient to express the Hamiltonian in the spinor basis:

$$\begin{aligned}\psi^{\dagger}_{a\mathbf{k}} &= (f^{\dagger}_{1+\mathbf{k}}, f^{\dagger}_{2-\mathbf{k}}, f^{\dagger}_{1+\mathbf{k}+\mathbf{Q}}, f^{\dagger}_{2-\mathbf{k}+\mathbf{Q}}), \\ \psi^{\dagger}_{b\mathbf{k}} &= (f^{\dagger}_{1-\mathbf{k}}, f^{\dagger}_{2+\mathbf{k}}, f^{\dagger}_{1-\mathbf{k}+\mathbf{Q}}, f^{\dagger}_{2+\mathbf{k}+\mathbf{Q}}),\end{aligned} \tag{10}$$

where it factorizes into two Kramers degenerate (a,b) $4\otimes 4$ blocks. The generally two-component order parameter is given by $\boldsymbol{\phi} = (\phi_x, \phi_y)$ (with ordering wave vector $\mathbf{Q}$ now suppressed). The resulting quasiparticle energies are the eigenvalues of $\tilde{h}_{\mathbf{k}} = (h_{\mathbf{k}} - \omega I) = \tilde{h}_{a\mathbf{k}}\otimes\tilde{h}_{b\mathbf{k}}$. The $4\otimes 4$

Hamiltonian blocks in spinor basis are given by

$$\tilde{h}_{a\mathbf{k}} = \begin{pmatrix} \hat{a}_{\mathbf{k}} & \hat{\lambda}_a \\ \hat{\lambda}_a & \hat{a}_{\mathbf{k}+\mathbf{Q}} \end{pmatrix}; \quad \hat{a}_{\mathbf{k}} = \begin{pmatrix} \tilde{A}_{1\mathbf{k}} & D_{\mathbf{k}} \\ D^*_{\mathbf{k}} & \tilde{A}_{2\mathbf{k}} \end{pmatrix}; \\ \hat{\lambda}_a = \begin{pmatrix} 0 & -\kappa(\phi_x - \mathrm{i}\phi_y) \\ -\kappa(\phi_x + \mathrm{i}\phi_y) & 0 \end{pmatrix}, \tag{11}$$

with $\tilde{A}_{\alpha\mathbf{k}} = A_{\alpha\mathbf{k}} - \omega$ where $A_{\alpha\mathbf{k}}$ and $D_{\mathbf{k}}$ are defined in Appendix. The secular equation $|\tilde{h}_{a\mathbf{k}}| = 0$ for the eigenvalues is obtained as

$$|D_{\mathbf{k}}|^2(\tilde{A}_{1\mathbf{k}}\tilde{A}_{2\mathbf{k}} + \tilde{A}_{1\mathbf{k}+\mathbf{Q}}\tilde{A}_{2\mathbf{k}+\mathbf{Q}}) - [(\tilde{A}_{1\mathbf{k}}\tilde{A}_{2\mathbf{k}+\mathbf{Q}} - \kappa^2|\boldsymbol{\phi}|^2) \\ \times (\tilde{A}_{2\mathbf{k}}\tilde{A}_{1\mathbf{k}+\mathbf{Q}} - \kappa^2|\boldsymbol{\phi}|^2) + |D_{\mathbf{k}}|^4] - 2\kappa^2|\boldsymbol{\phi}|^2\tilde{D}_{\mathbf{k}} = 0, \tag{12}$$

where we defined the real function

$$\tilde{D}_{\mathbf{k}} = \tfrac{1}{2}\left(c^2 D^2_{\mathbf{k}} + c^{*2} D^{*2}_{\mathbf{k}}\right),$$

and $c = (\hat{\phi}_x + i\hat{\phi}_y)$ with $|c|^2 = 1$. Solving this fourth-order equation leads to the closed solution for the four HO quasiparticle bands ($i = 1$–4) valid for general $\mathbf{k}$ ($\pm$ chosen independently):

$$\varepsilon_{i\mathbf{k}} = \varepsilon^{\pm}_{1,2}(\mathbf{k}) = A^{\perp}_{\mathbf{k}} \pm \left(\omega_0^2 \pm \tilde{\omega}_0^2\right)^{\frac{1}{2}}, \\ \omega_0^2 = A^{z2}_{\mathbf{k}} + \Delta^{\perp 2}_{\mathbf{k}} + |D_{\mathbf{k}}|^2 + \kappa^2|\boldsymbol{\phi}|^2, \\ \tilde{\omega}_0^2 = 2\left[A^{z2}_{\mathbf{k}}\left(\Delta^{\perp 2}_{\mathbf{k}} + |D_{\mathbf{k}}|^2\right) + \kappa^2|\boldsymbol{\phi}|^2\zeta_{\mathbf{k}}\right]^{\frac{1}{2}}, \tag{13}$$

or, explicitly ($i = \pm,1,2$) $\equiv$ ($i = 1-4$)

$$\varepsilon_{i\mathbf{k}} = \varepsilon^{\pm}_{1,2}(\mathbf{k}) = A^{\perp}_{\mathbf{k}} \pm \left\{\left(A^{z2}_{\mathbf{k}} + \Delta^{\perp 2}_{\mathbf{k}} + |D_{\mathbf{k}}|^2 + \kappa^2|\boldsymbol{\phi}|^2\right)\right. \\ \left. \pm 2\left[A^{z2}_{\mathbf{k}}\left(\Delta^{\perp 2}_{\mathbf{k}} + |D_{\mathbf{k}}|^2\right) + \kappa^2|\boldsymbol{\phi}|^2\zeta_{\mathbf{k}}\right]^{\frac{1}{2}}\right\}^{\frac{1}{2}}, \tag{14}$$

where on the left-hand side (l.h.s.) $\pm$ corresponds to the second and 1,2 to the first $\pm$ on the right-hand side (r.h.s.), respectively. Here, we defined $|\boldsymbol{\phi}| = (\phi_x^2 + \phi_y^2)^{\frac{1}{2}}$ as the order parameter amplitude with $\hat{\boldsymbol{\phi}} = \boldsymbol{\phi}/|\boldsymbol{\phi}| = (\hat{\phi}_x, \hat{\phi}_y)$ and $A^{z,\perp}_{\mathbf{k}}$, $\Delta^{\perp}_{\mathbf{k}}$ and $D_{\mathbf{k}}$ are given in Appendix. Furthermore, with $D_{\mathbf{k}} = D'_{\mathbf{k}} + i\,D''_{\mathbf{k}}$ we introduce the azimuthal function $\zeta_{\mathbf{k}}$, which leads to the breaking of fourfold C_4 symmetry in the HO phase. Its general form is given by

$$\zeta_{\mathbf{k}} = \tfrac{1}{2}(|D_{\mathbf{k}}|^2 - \tilde{D}_{\mathbf{k}}) \\ = \tfrac{1}{2}\left[{D'_{\mathbf{k}}}^2 + {D''_{\mathbf{k}}}^2 + (D'_{\mathbf{k}}\hat{\phi}_y + D''_{\mathbf{k}}\hat{\phi}_x)^2 - (D'_{\mathbf{k}}\hat{\phi}_x - D''_{\mathbf{k}}\hat{\phi}_y)^2\right]. \tag{15}$$

In the normal state where $\zeta_{\mathbf{k}} = \frac{1}{2}|D_{\mathbf{k}}|^2$, the C_4 symmetry is preserved. This is no longer true in the HO phase due to the terms $\sim\hat{\phi}_{x,y}$. In the context of a Landau expansion of the free energy below T_{HO}, it is concluded that only phases $\hat{\boldsymbol{\phi}} = (\hat{\phi}_x, \hat{\phi}_y)$ are stable where both components have the same modulus $(\hat{\phi}_x, \pm\hat{\phi}_y) = \frac{1}{\sqrt{2}}(1, \pm 1)$ denoted by $E_-(1,1)$ and $E_-(1,\bar{1})$ or one of the component vanishes $(\hat{\phi}_x, \hat{\phi}_y) = (1,0),(0,1)$, denoted by $E_-(1,0)$ and $E_-(0,1)$. In each case, the two possibilities are two different domains of the same phase. The single component phase has been ruled out by torque experiments [14,19] therefore we will only consider the two component phase in the following. We get

$$E_-(1,1): \zeta_{\mathbf{k}} = \frac{1}{2}(D'_{\mathbf{k}} + D''_{\mathbf{k}})^2 \\ = 32t_{12}^2 \cos^2\frac{a}{2}k_x \sin^2\frac{a}{2}k_y \sin^2\frac{c}{2}k_z, \\ E_-(1,\bar{1}): \zeta_{\mathbf{k}} = \frac{1}{2}(D'_{\mathbf{k}} - D''_{\mathbf{k}})^2 \\ = 32t_{12}^2 \sin^2\frac{a}{2}k_x \cos^2\frac{a}{2}k_y \sin^2\frac{c}{2}k_z. \tag{16}$$

This (positive) function breaks fourfold C_4 rotational symmetry under a coordinate rotation $\mathbf{k} \to \mathbf{k}'$ by $\pi/2$ with $k'_x = k_y$, $k'_y = -k_x$. Therefore the in-plane symmetry is reduced to twofold rotations C_2 generally since $\zeta_{-\mathbf{k}} = \zeta_{\mathbf{k}}$. The different domains correspond to a $\pi/2$ rotation of $\mathbf{k}$ and therefore to a relative $\pi/2$- shift of the fourfold symmetry breaking effects [14]. In the following, we will mostly discuss the $E_-(1,1)$ domain of the two component phase. We note that the C_4 symmetry breaking, due to terms $\sim\hat{\phi}_{x,y}$ in $\zeta_{\mathbf{k}}$, is directly tied to the interorbital hopping t_{12}, because the order parameter is an interorbital electron hole condensate. Therefore it is absent for $k_z = 0$.

The second 4×4 block in Eq. (9), $\tilde{h}_{b\mathbf{k}}$, is obtained from $\tilde{h}_{a\mathbf{k}}$ by replacing $\hat{a}_{\mathbf{k}} \to \hat{b}_{\mathbf{k}}$ as obtained from $D_{\mathbf{k}} \to -D^*_{\mathbf{k}}$ and in addition replacing $\hat{\lambda}_a \to \hat{\lambda}^{\dagger}_a = \hat{\lambda}_b$. Since $|\tilde{h}_{b\mathbf{k}}| \equiv |\tilde{h}_{a\mathbf{k}}|$ the resulting quasiparticle dispersion from $|\tilde{h}_{b\mathbf{k}}| = 0$ is identical to $\omega^{\pm}_{1,2}(\mathbf{k})$ in Eq. (14). Therefore, altogether, each of these four branches (due to two orbitals and the unit cell doubling by ordering vector $\mathbf{Q}$) is in addition twofold degenerate. This degeneracy is due to the invariance under combined time reversal and translation by $\mathbf{Q}$ (under the presence of inversion symmetry), therefore the a,b equivalence is an effective Kramers degeneracy not lifted by the antiferrotype order, although time reversal symmetry itself is broken. This is similar to the quasiparticle bands in the itinerant 2D antiferromagnet where the same symmetry also leads to a Kramers-type degeneracy of these bands reconstructed by the AF order parameter [25].

B. Hexadecapole A_{2+} phase

The order parameter ϕ_z of this phase [Eq. (8)] is nondegenerate. Similar to the previous case, the full Hamiltonian may be given in block form as in Eq. (11), but with a different spinor basis and a molecular field part: we now use the reordered basis (the Kramers index in the last pair in a,b is interchanged):

$$\psi^{\dagger}_{a\mathbf{k}} = (f^{\dagger}_{1+\mathbf{k}}, f^{\dagger}_{2-\mathbf{k}}, f^{\dagger}_{1-\mathbf{k}+\mathbf{Q}}, f^{\dagger}_{2+\mathbf{k}+\mathbf{Q}}), \\ \psi^{\dagger}_{b\mathbf{k}} = (f^{\dagger}_{1-\mathbf{k}}, f^{\dagger}_{2+\mathbf{k}}, f^{\dagger}_{1+\mathbf{k}+\mathbf{Q}}, f^{\dagger}_{2-\mathbf{k}+\mathbf{Q}}), \tag{17}$$

then we obtain

$$\tilde{h}_{a\mathbf{k}} = \begin{pmatrix} \hat{a}_{\mathbf{k}} & \hat{\lambda}_a \\ \hat{\lambda}^{\dagger}_a & \hat{a}^*_{\mathbf{k}+\mathbf{Q}} \end{pmatrix}; \quad \hat{a}_{\mathbf{k}} = \begin{pmatrix} \tilde{A}_{1\mathbf{k}} & D_{\mathbf{k}} \\ D^*_{\mathbf{k}} & \tilde{A}_{2\mathbf{k}} \end{pmatrix}; \\ \hat{\lambda}_a = \begin{pmatrix} 0 & -i\kappa\phi_z \\ -i\kappa\phi_z & 0 \end{pmatrix}. \tag{18}$$

The second block $\tilde{h}_{b\mathbf{k}}$ is obtained from $\tilde{h}_{a\mathbf{k}}$ by replacing $\hat{a}_{\mathbf{k}} \to \hat{b}_{\mathbf{k}}$ through $D_{\mathbf{k}} \to -D^*_{\mathbf{k}}$ and in addition $\hat{\lambda}_a \to -\hat{\lambda}_a = \hat{\lambda}_b$. The secular equation $|\tilde{h}_{a\mathbf{k}}| = 0$ is similar to Eq. (12):

$$|D_{\mathbf{k}}|^2(\tilde{A}_{1\mathbf{k}}\tilde{A}_{2\mathbf{k}} + \tilde{A}_{1\mathbf{k}+\mathbf{Q}}\tilde{A}_{2\mathbf{k}+\mathbf{Q}}) - [(\tilde{A}_{1\mathbf{k}}\tilde{A}_{2\mathbf{k}+\mathbf{Q}} - \kappa^2|\phi_z|^2) \times (\tilde{A}_{2\mathbf{k}}\tilde{A}_{1\mathbf{k}+\mathbf{Q}} - \kappa^2|\phi_z|^2) + |D_{\mathbf{k}}|^4] - 2\kappa^2|\phi_z|^2|D_{\mathbf{k}}|^2 = 0. \tag{19}$$

Again, the four quasiparticle bands ($i = 1-4$) in the A_{2+} HO phase may be obtained in closed form as

$$\begin{aligned} \varepsilon_{i\mathbf{k}} &= \varepsilon^{\pm}_{1,2}(\mathbf{k}) = A^{\perp}_{\mathbf{k}} \pm \left(\omega_0^2 \pm \tilde{\omega}_0^2\right)^{\frac{1}{2}}, \\ \omega_0^2 &= A^{z2}_{\mathbf{k}} + \Delta^{\perp 2}_{\mathbf{k}} + |D_{\mathbf{k}}|^2 + \kappa^2|\phi_z|^2, \\ \tilde{\omega}_0^2 &= 2\left|A^z_{\mathbf{k}}\right|\left[\Delta^{\perp 2}_{\mathbf{k}} + |D_{\mathbf{k}}|^2\right]^{\frac{1}{2}}, \end{aligned} \tag{20}$$

or, explicitly ($i = \pm,1,2$) $\equiv$ ($i = 1-4$)

$$\varepsilon_{i\mathbf{k}} = E^{\pm}_{1,2}(\mathbf{k}) = A^{\perp}_{\mathbf{k}} \pm \sqrt{A^{z2}_{\mathbf{k}} + \Delta^{\perp 2}_{\mathbf{k}} + |D_{\mathbf{k}}|^2 + \kappa^2|\phi_z|^2 \pm 2|A^z_{\mathbf{k}}|\sqrt{\Delta^{\perp 2}_{\mathbf{k}} + |D_{\mathbf{k}}|^2}}. \tag{21}$$

The four branches from $|\tilde{h}_{b\mathbf{k}}| = 0$ are identical to those of $|\tilde{h}_{a\mathbf{k}}| = 0$ leading to a Kramers degeneracy similar as before (for A_{2+}, time reversal symmetry is already preserved by itself). The result in Eq. (21) is obtained from the E_- case dispersion of Eq. (14) formally by replacing $|\boldsymbol{\phi}| \to |\phi_z|$ and $\zeta_{\mathbf{k}} \to 0$. Therefore, due to the nondegeneracy of A_{2+}, which implies $|\phi_z|^2$ transforming like $A_{2+} \otimes A_{2+} = A_{1+}$, there is no term in the dispersion that breaks the fourfold rotational symmetry (and also not the in-plane reflection symmetry). This should give an important distinction in the QPI spectrum of the two phases.

C. Dispersion in special cases for E_- and A_{2+}

We also discuss some special and limiting cases for the dispersion for greater clarity. In the E_- phase, we have

$$\begin{aligned} \boldsymbol{\phi} = 0 &: \varepsilon^{\pm}_{1,2}(\mathbf{k}) = A^{\perp}_{\mathbf{k}} \pm A^z_{\mathbf{k}} \pm \sqrt{\Delta^{\perp 2}_{\mathbf{k}} + |D_{\mathbf{k}}|^2}, \\ D_{\mathbf{k}} = 0\ (k_z = 0) &: \varepsilon^{\pm}_{1,2}(\mathbf{k}) = A^{\perp}_{\mathbf{k}} \pm \sqrt{\left(A^z_{\mathbf{k}} \pm \Delta^{\perp}_{\mathbf{k}}\right)^2 + \kappa^2|\boldsymbol{\phi}|^2}, \\ D_{\mathbf{k}} = 0;\ \boldsymbol{\phi} = 0 &\ :\ \varepsilon^{\pm}_{1,2}(\mathbf{k}) = A^{\perp}_{\mathbf{k}} \pm A^z_{\mathbf{k}} \pm \Delta^{\perp}_{\mathbf{k}}. \end{aligned} \tag{22}$$

Note that the $\pm$ signs are chosen in arbitrary combination to give four bands (which are in addition twofold Kramers degenerate). The first equation describes quasiparticle bands in the para phase for general $\mathbf{k}$, the second in the ordered phase for in-plane wave vector and the last one for both conditions satisfied. Taking into account $A^z_{\mathbf{k}+\mathbf{Q}} = -A^z_{\mathbf{k}}$, the second equation is equivalent to the result in Ref. [12] in the Brillouin zone of the ordered phase. These special cases are described by identical dispersions for the A_{2+} phase when we replace $|\boldsymbol{\phi}| \to \phi_z$ in the second equation. The other equations refer to the para phase. Due to this identity, the reconstructed HO FS cuts with $k_z = 0$ are the same for both phases because then $\zeta_{\mathbf{k}} = 0$ for E_-. In order to see the difference between E_- and A_{2+}, we have to consider cuts with $|k_z| > 0$ where the fourfold symmetry breaking through nonzero $\zeta_{\mathbf{k}}$ appears.

V. GREEN'S FUNCTION, QUASIPARTICLE DOS, AND QPI SPECTRUM IN HO PHASE

To calculate the QPI spectrum for both HO models we need the Green's function $G_{\mathbf{k}} = G_{a\mathbf{k}} \otimes G_{b\mathbf{k}}$ with $G_{\gamma\mathbf{k}} = (i\omega_n 1 - h_{\gamma\mathbf{k}})^{-1}$ ($\gamma = a,b$). The Green's function matrices will be diagonal in the basis of the four quasiparticle eigenvectors ($i,j = 1,4$) of $h^{a,b}_{\mathbf{k}}$, which form the columns of the unitary transformation $U_{\gamma\mathbf{k}}$ in

$$h'_{\gamma\mathbf{k}} = U_{\gamma\mathbf{k}} h_{\gamma\mathbf{k}} U^{\dagger}_{\gamma\mathbf{k}}; \quad \{h'_{\gamma\mathbf{k}}\}_{ij} = \varepsilon_{i\mathbf{k}}\delta_{ij}, \tag{23}$$

where $\varepsilon_{i\mathbf{k}}$ has Kramers degeneracy with respect to γ. The primed spinors $\psi'_{\gamma\mathbf{k}} = U_{\gamma\mathbf{k}}\psi_{\gamma\mathbf{k}}$ corresponding to the eigenvectors satisfy the canonical anticommutation relations. In this primed basis, we obtain the Green's functions

$$G'_{\gamma\mathbf{k}}(i\omega_n) = (i\omega_n 1 - h'_{\gamma\mathbf{k}})^{-1}, \tag{24}$$

therefore we have

$$G'_{\gamma\mathbf{k}}(i\omega_n)_{ij} = \frac{\delta_{ij}}{(i\omega_n - \varepsilon_{i\mathbf{k}})}, \tag{25}$$

where $\varepsilon_{i\mathbf{k}}$ are the exact solutions for the quasiparticle bands in Eqs. (14) or (21). The Green's function does not depend on γ. Then we may obtain the quasiparticle DOS (per Kramers pseudospin degree) as

$$\begin{aligned} N(\omega) &= -\frac{1}{\pi}\mathrm{Im}\frac{1}{N}\sum_{i\mathbf{k}}\left(\frac{1}{i\omega_n - \varepsilon_{i\mathbf{k}} + i\eta}\right)_{i\omega_n \to \omega + i\eta} \\ &= -\frac{1}{\pi}\mathrm{Im}\frac{1}{N}\sum_{\mathbf{k}}\frac{4\omega_{\mathbf{k}}\left(\omega^2_{\mathbf{k}} - \omega_0^2\right)}{\left(\omega^2_{\mathbf{k}} - \omega_0^2\right)^2 - \left(\tilde{\omega}_0^2\right)^2}, \end{aligned} \tag{26}$$

where the sum over band index i has been carried out explicitly in the second expression. Here, $\omega_{\mathbf{k}} = \omega - A^{\perp}_{\mathbf{k}} + i\eta$ with $\eta \to 0$. The evolution of the HO gap in $N(\omega)$ is shown in Fig. 2(d).

The quasiparticle interference spectrum is the Fourier transform of the change in local density of states introduced by scattering from dilute impurities on the surface [26]. It may be calculated within the t-matrix theory of scattering. We assume a scattering potential strength $V_0 \ll \phi$ that is small compared to the hidden order gap (Sec. VII). Then it is reasonable to express the impurity Hamiltonian directly within the basis of quasiparticles in the HO state. We take the simplest form of a nonmagnetic momentum- and orbital- independent scattering excluding interband processes. In the primed (HO) quasiparticle basis, it is written as

$$H_{\mathrm{imp}} = \frac{V_0}{N}\sum_{\mathbf{kq}}[\psi'^{\dagger}_{a\mathbf{k}+\mathbf{q}}\psi'_{a\mathbf{k}} + \psi'^{\dagger}_{b\mathbf{k}+\mathbf{q}}\psi'_{b\mathbf{k}}]. \tag{27}$$

For $\omega \ll \phi$ and sufficiently small V_0 as defined above, the QPI spectrum may be treated in the Born approximation for

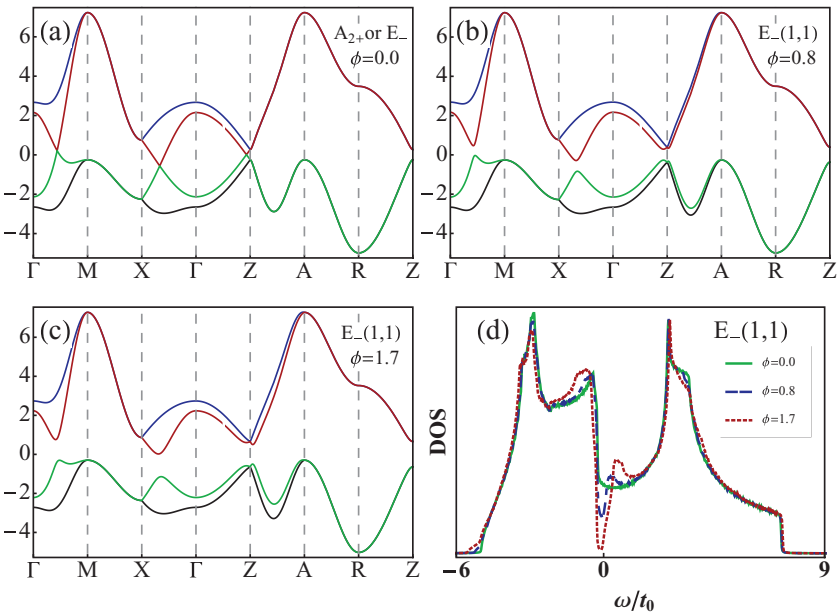

FIG. 2. (Color online) Dispersion along the st BZ path $\Gamma(0,0,0)$, $M(\frac{1}{2},\frac{1}{2},0)$; $X(0,\frac{1}{2},0)$; $Z(0,0,\frac{1}{2})$; $A(\frac{1}{2},\frac{1}{2},\frac{1}{2})$; and $R(0,\frac{1}{2},\frac{1}{2})$. (a) Effective f bands in the para phase. (b) and (c) Reconstructed quasiparticle bands in the $E_-(1,1)$ HO phase for $\phi = 0.8$ and 1.7. The gapping of quasiparticle dispersion at $\mathbf{k}$ points connected by the nesting vector $\mathbf{Q} = (0,0,1)$ (r.l.u.) can be clearly seen. (d) DOS with evolution of HO gap with ϕ [also Fig. 4(c)]. Here and in subsequent figures, we define $\phi = |\phi_z^{\mathbf{Q}}|$ or $|\boldsymbol{\phi}^{\mathbf{Q}}|$ in units of $t_0 = 6.66$ meV.

the scattering [27] leading to a local DOS modification (per Kramers pseudospin) given by

$$\delta N(\mathbf{q},\omega) = \frac{-V_0}{2\pi N}\mathrm{Im}\sum_{\gamma\mathbf{k}} tr[G'_{\gamma\mathbf{k}}(\mathrm{i}\omega_n)G'_{\gamma\mathbf{k}-\mathbf{q}}(\mathrm{i}\omega_n)]_{\mathrm{i}\omega_n\to\omega+\mathrm{i}\eta}. \tag{28}$$

The trace may easily be evaluated and by defining $\delta N(\mathbf{q},\omega) = V_0\Lambda(\mathbf{q},\omega)$ we obtain the final QPI spectrum as

$$\Lambda(\mathbf{q},\mathrm{i}\omega_n) = -\frac{1}{\pi}\mathrm{Im}\frac{1}{N}\sum_{i\mathbf{k}}(\mathrm{i}\omega_n - \varepsilon_{i\mathbf{k}})^{-1}(\mathrm{i}\omega_n - \varepsilon_{i\mathbf{k}-\mathbf{q}})^{-1}. \tag{29}$$

This expression for the QPI spectrum is valid for both E_- and A_{2+} type HO, using the quasiparticle dispersions $\varepsilon_{i\mathbf{k}}$ given in Eqs. (14) and (21) for E_- and A_{2+} HO, respectively.

The $\mathbf{q}$ vector in $\Lambda(\mathbf{q},\mathrm{i}\omega_n)$ is a 2D surface vector. However, the integration over $\mathbf{k}$ has to be performed over the full 3D BZ of URu_2Si_2 since its FS has a 3D character and the k_z component is not preserved in tunneling due to the surface. Nevertheless, as shown in the example of the $d_{x^2-y^2}$-wave superconductor $CeCoIn_5$ [8], it is instructive to consider the QPI spectrum for each k_z slice of the FS separately for the presence of characteristic features of the equal quasiparticle energy surface in the HO phase. Then, the summation over k_z is performed to see which of those features survive in the total QPI spectrum observed in experiment.

VI. QPI IN THE CHIRAL SUPERCONDUCTING PHASE EMBEDDED IN HIDDEN ORDER

At $T_c = 1.45$ K, far below $T_{\mathrm{HO}} = 17.5$ K, URu_2Si_2 becomes superconducting. As a function of pressure, this embedding in the HO phase is maintained up to the critical pressure of $p_c \simeq 0.7$ kbar where both superconductivity and hidden order vanish [28]. Therefore one may conjecture that HO is a necessary condition for SC to appear in this compound. Various experiments like field-angle dependent thermal conductivity [7,29] and specific heat [30] measurements have been interpreted in terms of a chiral d-wave gap symmetry that has line and point nodes. Since the investigation of gap structures in heavy fermion superconductors by QPI has recently been successfully demonstrated for $CeCoIn_5$ [8–10], it is worthwhile to perform a theoretical analysis of the predicted QPI pattern in the proposed chiral d-wave gap. So far, experimentally, the QPI investigations [11] have been limited to the hidden order phase for $T_c < T \ll T_{\mathrm{HO}}$.

We start from the reasonable assumption ($T_c \ll T_{\mathrm{HO}}$) that the SC order parameter is formed by pairing of reconstructed quasiparticles of the HO phase whose dispersion is given by Eqs. (14) and (21). They are described by the Nambu spinors $\Psi'^{i\dagger}_{\mathbf{k}} = (\psi'^{i\dagger}_{a\mathbf{k}}, \psi'^{i}_{b\bar{\mathbf{k}}})$ with the definition $\bar{\mathbf{k}} = -\mathbf{k}$ and with $i = 1-4$ denoting one of the four HO quasiparticle bands, which are twofold (a,b) Kramers degenerated. Therefore the indices $a\mathbf{k}$ and $b\bar{\mathbf{k}}$ refer to time reversed states with opposite quasiparticle Kramers pseudospins (a,b) and momenta $(\mathbf{k},\bar{\mathbf{k}})$. The mean-field Hamiltonian for the singlet pairing of the effective pseudospin states of HO quasiparticles is then

$$\begin{aligned} H_{\mathrm{MF}} &= \sum_{\mathbf{k}i}\begin{pmatrix}\psi'^{i\dagger}_{a\mathbf{k}} & \psi'^{i}_{b\bar{\mathbf{k}}}\end{pmatrix}\begin{pmatrix}\varepsilon_{i\mathbf{k}} & \Delta_{i\mathbf{k}}\\ \Delta^*_{i\mathbf{k}} & -\varepsilon_{i\mathbf{k}}\end{pmatrix}\begin{pmatrix}\psi'^{i}_{a\mathbf{k}}\\ \psi'^{i\dagger}_{b\bar{\mathbf{k}}}\end{pmatrix} \\ &= \sum_{\mathbf{k}i}\Psi'^{i\dagger}_{\mathbf{k}}\hat{h}^i_{\mathbf{k}}\Psi'^{i}_{\mathbf{k}}, \end{aligned} \tag{30}$$

where $\Delta_{i\mathbf{k}}$ is the singlet gap function discussed below. The Green's function matrix is then given by $\hat{G}^i_0(\mathbf{k},\mathrm{i}\omega_n) = (\mathrm{i}\omega_n - \hat{h}^i_{\mathbf{k}})^{-1}$, which has the normal (diagonal) and anomalous (off-diagonal condensate) elements

$$\begin{aligned} G^i_0(\mathbf{k},\mathrm{i}\omega_n) &= \frac{\mathrm{i}\omega_n + \varepsilon_{i\mathbf{k}}}{(\mathrm{i}\omega_n)^2 - E^2_{i\mathbf{k}}}, \\ F^i_0(\mathbf{k},\mathrm{i}\omega_n) &= \frac{\Delta_{\mathbf{k}}}{(\mathrm{i}\omega_n)^2 - E^2_{i\mathbf{k}}}. \end{aligned} \tag{31}$$

Here, $E_{i\mathbf{k}} = \sqrt{\varepsilon^2_{i\mathbf{k}} + |\Delta_{\mathbf{k}}|^2}$ are the SC quasiparticle energies where we assumed the same gap function $\Delta_{i\mathbf{k}} \equiv \Delta_{\mathbf{k}}$ for each

band. Considering only nonmagnetic weak impurity scattering as before, the QPI spectrum in the coexisting HO + SC state is then given by

$$\Lambda(\mathbf{q},i\omega_n) = -\frac{1}{\pi}\mathrm{Im}\frac{1}{N}\sum_{i\mathbf{k}}\big[G_0^i(\mathbf{k},i\omega_n)G_0^i(\mathbf{k}-\mathbf{q},i\omega_n) - F_0^i(\mathbf{k},i\omega_n)F_0^{i*}(\mathbf{k}-\mathbf{q},i\omega_n)\big], \quad (32)$$

leading to the final expression

$$\Lambda(\mathbf{q},i\omega_n) = -\frac{1}{\pi}\mathrm{Im}\frac{1}{N}\sum_{i\mathbf{k}}\frac{(i\omega_n+\varepsilon_{i\mathbf{k}})(i\omega_n+\varepsilon_{i\mathbf{k}-\mathbf{q}})-\Delta_{\mathbf{k}}\Delta^*_{\mathbf{k}-\mathbf{q}}}{\big[(i\omega_n)^2-E^2_{i\mathbf{k}}\big]\big[(i\omega_n)^2-E^2_{i\mathbf{k}-\mathbf{q}}\big]}. \quad (33)$$

For $\Delta_{\mathbf{k}}=0$, it reduces to the expression for the normal state with HO in Eq. (29). For the explicit calculation of $\Lambda(\mathbf{q},i\omega_n)$ in the coexisting HO + SC, we need a concrete model for the SC gap function in addition to the HO models defined in Eqs. (6) and (8). As mentioned above, the chiral d-wave gap function has been proposed from thermal transport and specific heat results. Its explicit form is

$$\Delta_{\mathbf{k}} = \Delta_0 \sin\frac{c}{2}k_z\left[\sin\frac{a}{2}(k_x+k_y)+i\sin\frac{a}{2}(k_x-k_y)\right], \quad (34)$$

with an absolute value $|\Delta_{\mathbf{k}}|$ that is given by

$$|\Delta_{\mathbf{k}}|^2 = 2\Delta_0^2\sin^2\frac{c}{2}k_z\left[\sin^2\frac{a}{2}k_x\cos^2\frac{a}{2}k_y + \cos^2\frac{a}{2}k_x\sin^2\frac{a}{2}k_y\right].$$

This gap function has line nodes in the tetragonal plane $k_z=0,\pm 2\pi/c$, which are equivalent in the folded st BZ. Furthermore, it has additional point nodes at locations $k_x=k_y=0$. This may lead to interesting consequences for the QPI spectrum: for a small bias voltage $\omega \ll \Delta_0$, the surfaces $E_{i\mathbf{k}}=\omega$ have essentially $k_z\simeq 0$ and are unchanged from the non-SC HO state. Consequently, the QPI will essentially be only determined by the quasi-2D HO Fermi surface at $k_z=0$ shown in Fig. 1. Therefore the chiral SC gap opening in a way reveals the true HO characteristics in the QPI by reducing it to a 2D situation. However, this also means that one should expect a suppression of any difference in QPI for E_- and A_{2+} HO in the SC state because in the plane $k_z=0$ they have identical quasiparticle dispersion.

VII. NUMERICAL RESULTS AND DISCUSSION

Using the previous analysis, we may now predict all essential QPI spectral properties of the HO and the coexisting HO + SC phase. We first specify the numerical parameters. Those for the effective $5f$ bands of the para phase are cited in Appendix. The total quasiparticle bandwidth of the model is given by $W_{\mathrm{qp}}=12t_0$ according to Fig. 2(a) in units of Ref. [12]. The absolute scale is obtained by comparing with STM results for URu_2Si_2 [31] where $W_{\mathrm{qp}}\simeq 80$ meV leading to $t_0=6.66$ meV.

In the HO phase, the gap at nesting points is $\Delta_{\mathrm{HO}}=\phi/\sqrt{2}$. From Ref. [32], we have $\Delta_{\mathrm{HO}}=4.1$ meV or $\phi=5.8$ meV. With the smaller $T_{\mathrm{HO}}=16$ K for gap onset [32], this leads to a HO BCS ratio $2\Delta_{\mathrm{HO}}/kT_{\mathrm{HO}}=5.8$. Furthermore, we have $\Delta_{\mathrm{HO}}/W_{\mathrm{qp}}=5.1\times10^{-2}$. This sizable HO gap value is favorable for a clear structure formation in QPI. The corresponding maximum amplitude of HO is $\phi=7.25\times10^{-2}W_{\mathrm{qp}}$ or $\phi=0.87t_0$.

In the superconducting state, we have the average gap value from Ref. [33] with $2\Delta_0/kT_c=5.6$. With $T_c=1.45$ K, this means a SC gap amplitude of $\Delta_0=0.35$ meV, which is an order of magnitude smaller than the HO gap. Furthermore, we get $\Delta_0/W_{\mathrm{qp}}=0.44\times10^{-2}$ or $\Delta_0/t_0=0.05$. To enhance the QPI structures induced by SC state more clearly, we will also use a larger value for Δ_0.

First, we discuss basic characteristics of the para phase model Fermi surface (Fig. 1) and band structure [Fig. 2(a)], which was proposed by Rau and Kee [12]. In the unfolded para phase BZ, there is an electron sheet around Γ and a hole sheet around Z that have comparable sizes and large portions that are nested with $\mathbf{Q}=(0,0,1)$. In the folded BZ, the latter is projected to Γ, in a corresponding k_x-k_y–plane cut [Fig. 1(b)], the nested regions are around the crossing points. Therefore the FS sheets will break up around these crossings in the HO phase. The complementary k_x-k_z–plane cut is shown in Fig. 1(c). The band structure in the folded st BZ is shown in Fig. 2(a) and exhibits again the crossing of electronlike and holelike branches, e.g., along ΓX.

Turning on the HO parameter leads to a repulsion of bands at the crossing point, opening a gap locally [Figs. 2(b) and 2(c)]. This results in a sharp dip in the DOS at the Fermi level [Fig. 2(d)] as a function of increasing HO strength. Such drastic decrease in the quasiparticle DOS in the HO phase was indeed seen in transport measurements [34,35]. The Fermi surface reconstruction in the HO phase is shown in Fig. 3(a) in a 3D representation in the *folded* BZ [cf. Fig. 1(a) in the *unfolded* BZ]. The HO introduces a void in the formerly closed FS body at the Z points and slices the FS parallel to k_z at the crossing points of the nested sheets. In the corresponding k_x-k_y–plane cut [Fig. 3(b)], the formerly closed and rounded squarelike sheets [Fig. 1(b)] therefore break up into four smaller and four larger petal-like shapes. The smaller ones vanish when the HO parameter $\phi=|\boldsymbol{\phi}^{\mathbf{Q}}|$ or $|\phi_z^{\mathbf{Q}}|$ is increased still further. The k_x-k_z–plane cut in Fig. 3(c) in comparison with Fig. 1(c) shows again the vanishing of the FS around the Z point when the HO gap opens.

These main features are similar for both E_- and A_{2+} HO symmetries. However, one can identify subtle differences in the reconstructed FS. They are not present for $k_z=0$ cuts because in this case the HO reconstructed dispersions in Eqs. (14) and (21) are formally equivalent [second of Eq. (22)]. The difference appears in k_x-k_y–plane cuts for $|k_z|>0$ as shown in Figs. 4(a) and 4(b). For the $E_-(1,1)$ HO (a), clearly, the C_4 rotational symmetry of FS sheets is destroyed. The symmetry breaking to C_2 would be rotated by $\pi/2$ for the other $E_-(1,\bar{1})$ domain. This asymmetry is absent for the A_{2+} HO (b) where all petals still have the same size, preserving C_4 symmetry. Therefore the set of characteristic wave vectors connecting the tips of the petals, which should be seen in QPI will be different in the two cases. In Fig. 4(c), we present a

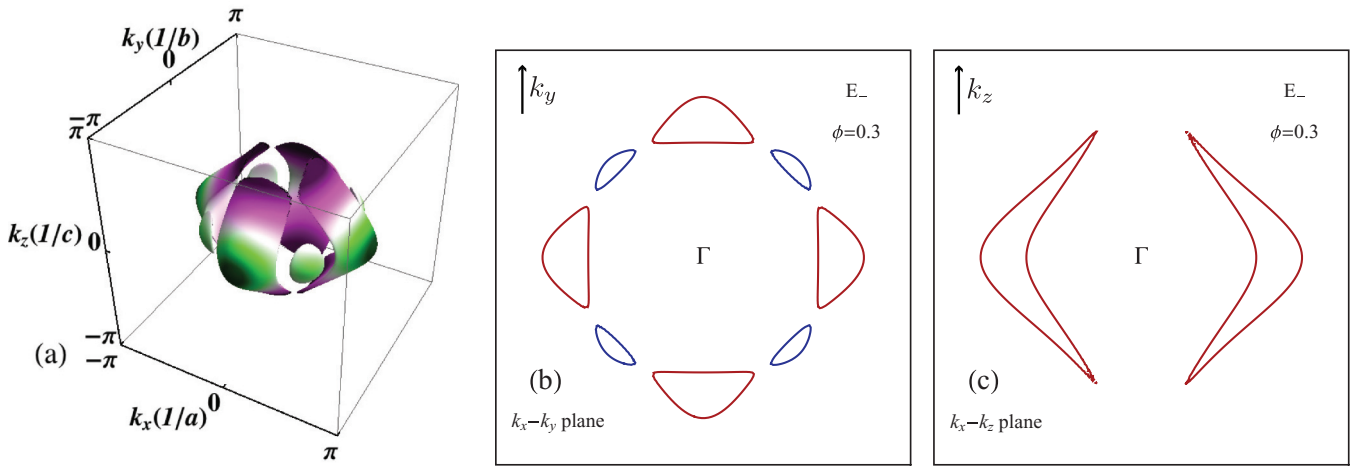

FIG. 3. (Color online) (a) Fermi surface sheets of URu_2Si_2 in the $E_-(1,1)$ HO phase in the reduced BZ (folded by $\mathbf{Q}$). The FS is reconstructed in $\mathbf{k}$-space regions connected by the nesting vector $\mathbf{Q} = (0,0,1)$ and breaks up into four larger and four smaller sheets (partly hidden). FS cuts in (b) the k_x-k_y plane and (c) the k_x-k_z plane. We note that the fourfold symmetry breaking of the E_- HO does not appear in (b) where $k_z = 0$ (cf. Fig. 4). The momentum range in (b) and (c) is given by $-\pi \leqslant k_i \leqslant \pi$.

zoomed DOS in the HO gap region, which shows that the DOS at the Fermi level is strongly reduced when HO develops. This agrees with the experimental observations [34,35].

Now, we discuss the main results of QPI calculations. As mentioned before, URu_2Si_2 is not an ideal case for the STM-QPI method due to its largely 3D electronic structure. In such a case we proceed in two steps [8]. First, we calculate the QPI spectrum of slices of a given k_z component for wave vectors in the tetragonal plane. This allows one to identify directly the effect of Fermi surface and hidden order on each contribution. For the total QPI spectrum that has to be compared with experiment, one must integrate over all slices of different k_z, then the question is how much of the characteristic Fermi surface and HO structures in the spectrum survive after the integration and can still be used as a diagnostic of the HO state. In all following figures, we show only the absolute value $|\Lambda(\mathbf{q},\omega)|$ of the QPI spectrum.

In Fig. 5, we show the FS cut and the corresponding QPI spectrum (absolute value) for the $k_z = 0$ slice and $\phi = 0.7t_0$, which is identical for both HO symmetries. It is the most important one because the $v^z_{i\mathbf{k}} = \partial\varepsilon_{i\mathbf{k}}/\partial k_z$ velocity components vanish for $k_z = 0$ [Fig. 3(a)] leading to a large resultant contribution with $k_z \approx 0$ neighboring slices. The characteristic intrasheet and intersheet scattering wave vectors of the HO reconstructed Fermi surface are shown in Fig. 5(a). They should reappear prominently in the calculated QPI spectrum of Fig. 5(b). Indeed, most of them can be clearly identified. As a whole, the reconstructed HO Fermi surface can be well recognized in the QPI image in Fig. 5(b) if one keeps in mind that in the latter the characteristic length of Fermi vectors k_F in Fig. 5(a) will be mapped to $2k_F$. This means that some of the features like the "petal" images produced by $\mathbf{q}_2^{a-c}$ scattering look inverted because they are folded back from the next BZ, leading to effective characteristic wave

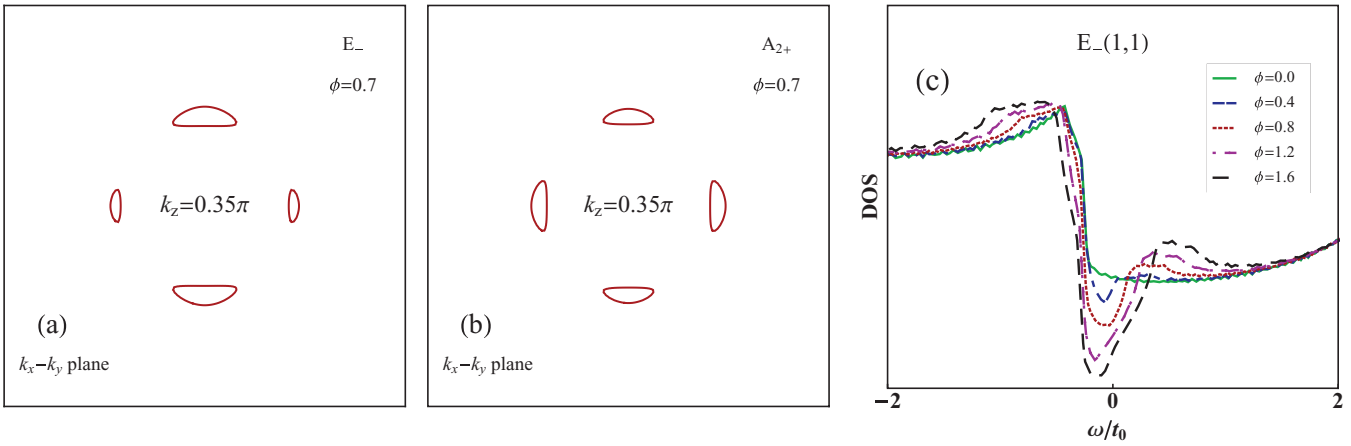

FIG. 4. (Color online) Comparison of reconstructed Fermi surface sheets of URu_2Si_2 for different HO symmetry in the k_x-k_y plane with $|k_z| = 0.35\pi$. (a) In the $E_-(1,1)$ phase, the breaking of fourfold rotational C_4 symmetry for $k_z \neq 0$ is obvious. Changing to $E_-(1,\bar{1})$ domain corresponds to $\pi/2$ rotation. (b) For A_{2+}, HO fourfold symmetry is preserved. (c) Zoomed DOS in the HO gap region for various ϕ. Charge carrier DOS is reduced to small values for large ϕ. Momentum range in (a) and (b) is given by $-\pi \leqslant k_i \leqslant \pi$.

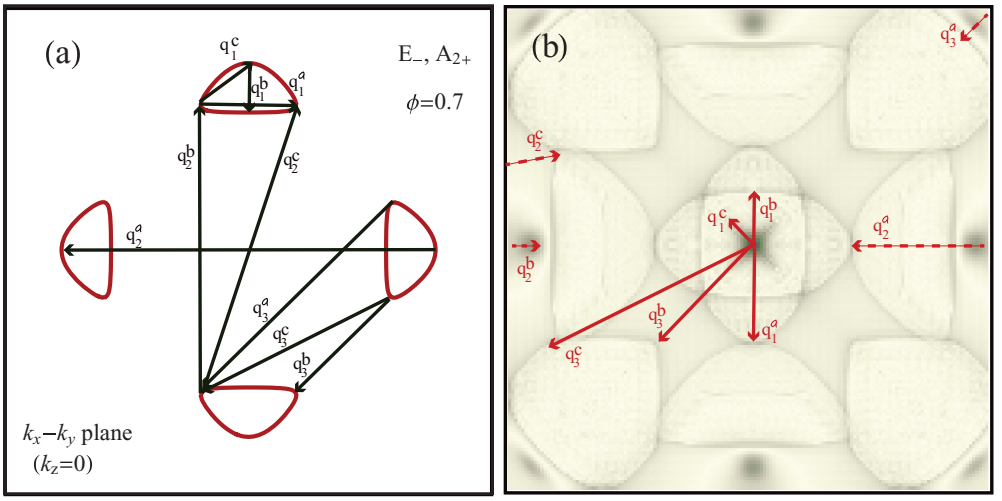

FIG. 5. (Color online) (a) Reconstructed HO Fermi surface ($\omega = 0$) for $\phi = 0.7$ (in units of t_0) in the k_x-k_y plane with $k_z = 0$ where E_-, A_{2+} are equivalent. The characteristic scattering wave vectors $\mathbf{q}_{1-3}^{a-c}$ for the QPI spectrum are indicated. (b) Partial QPI (absolute value) spectrum ($\omega = 0$) for $k_z = 0$ slice of the Fermi surface. All $\mathbf{q}_i^{\alpha}$ are present and the image of HO FS sheets that have doubled '$2k_F$' dimension is clearly visible. The momentum range is given by $-\pi \leqslant k_i \leqslant \pi$.

vectors $\mathbf{q}_2^{a-c} \rightarrow \mathbf{q}_2^{a-c} - \mathbf{K}$ [dashed arrows in Fig. 5(b)] with $\mathbf{K}$ denoting a reciprocal lattice vector.

The $k_z = 0$ slice QPI image in Fig. 5(b) is identical for E_- and A_{2+} HO and has the fourfold C_4 symmetry. For $|k_z| > 0$ slices, they should become distinct and the symmetry breaking for E_- QPI image should appear corresponding to the Fermi surface cut in Fig. 4(a). This happens gradually because the symmetry breaking term in Eqs. (14) and (16) behaves like $\zeta_{\mathbf{k}} \sim \sin^2 \frac{c}{2} k_z$. Thus for $k_z/(\pi/c) \ll 1$ the QPI image will be qualitatively as in Fig. 5(b). For larger k_z, it changes rapidly as seen in Fig. 6. The dimensions generally shrink because of the reduction of Fermi surface dimensions obvious from

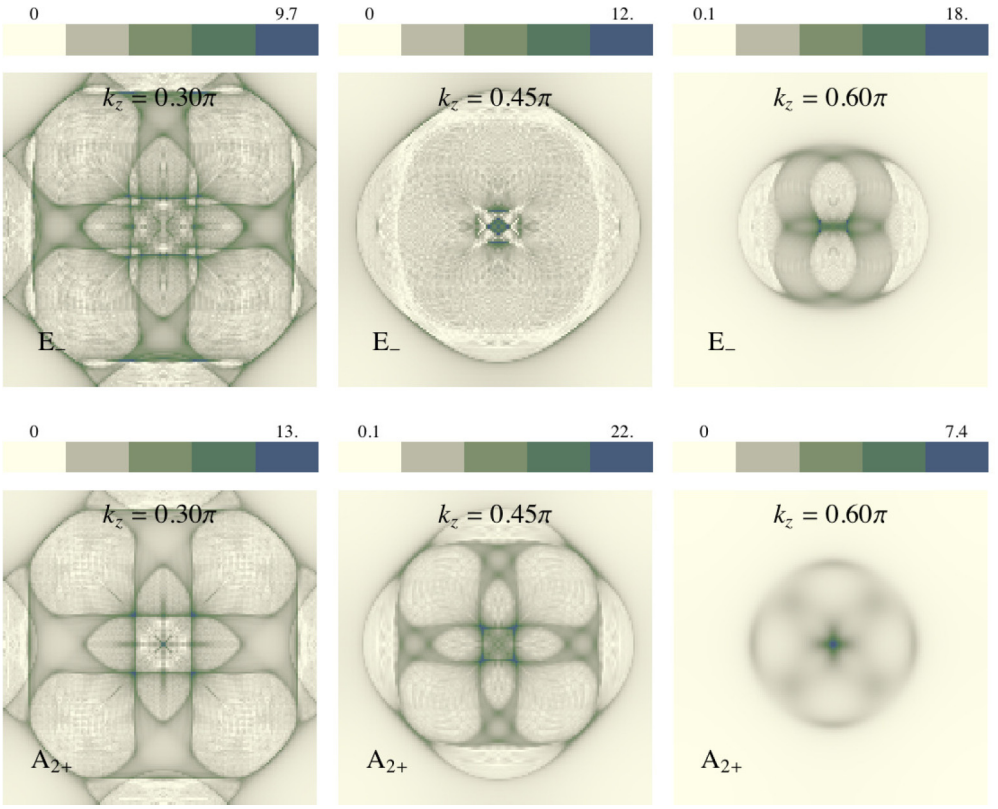

FIG. 6. (Color online) Partial QPI (absolute value) spectra ($\omega = 0.124 t_0$) for different $|k_z| > 0$ slices for E_- (first row) and A_{2+} (second row) HO. For larger k_z, distinct C_4 symmetry breaking due to the $\zeta_{\mathbf{k}}$ function in the dispersion of Eq. (14) appears for E_-, while C_4 is preserved for A_{2+}. (The momentum range is given by $-\pi \leqslant q_{x,y} \leqslant \pi$.)

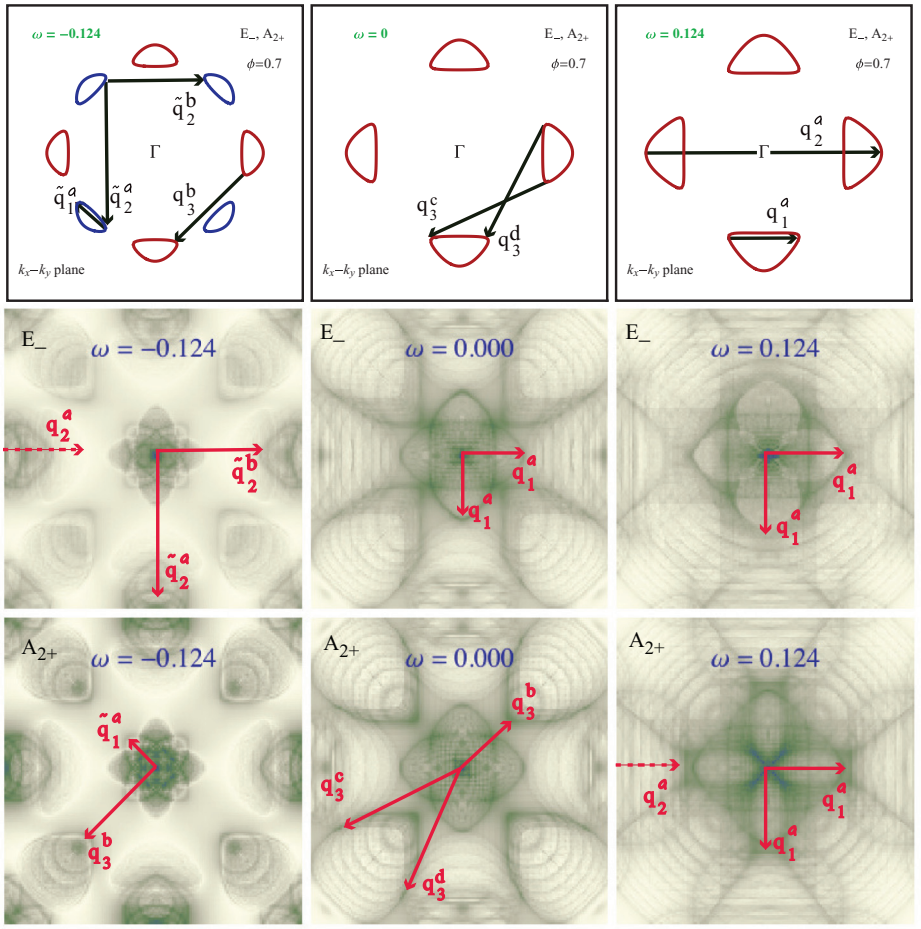

FIG. 7. (Color online) Constant energy surfaces ($\epsilon_{i\mathbf{k}} = \omega$) for $k_z = 0$ (top row, identical for both HO) and total QPI (absolute value) spectra ($\omega = 0, -0.124t_0, 0.124t_0$) for E_- (center row) and A_{2+} (bottom row) HO parameter. C_4 symmetry is preserved for A_{2+} while a distinct rotational symmetry breaking is still visible in the integrated QPI for E_-. Note that the latter is due to the $|k_z| > 0$ contributions not depicted in the top row. Dashed arrows denote an image folded back into the first BZ. The momentum range is given by $-\pi \leqslant k_i \leqslant \pi$.

Fig. 3(a). However, more importantly, while the A_{2+} image in Fig. 6 retains the fourfold symmetry for all k_z, the E_- image develops a twofold anisotropy for increasing k_z. This is already visible for $k_z = 0.3$ since the axis oriented lobes have different widths and the diagonal lobes are not completely symmetric. For even larger k_z, the structure of the E_- QPI image changes and develops a pronounced twofold symmetry, in contrast to the A_{2+} QPI image, which is perfectly C_4 symmetric for all slices.

The question is now how much of these intricate features in Figs. 5 and 6 for the individual slices will survive in the integrated QPI spectrum, which can be measured. It is shown in Fig. 7 for three frequencies (bias voltages) $\omega = 0, \pm 0.124t_0$ and E_- (second row) and A_{2+} (third row) HO with $\phi = 0.7t_0$. Note that the value of the bias voltage is still considerably smaller than the HO gap $\Delta_{\mathrm{HO}} = 0.62t_0$. The top row shows the spectral function (equal energy surfaces) in the three cases. While $\omega/t_0 = 0, 0.124$ are similar except for the larger sheet dimensions, the case for negative bias $\omega/t_0 = -0.124$ is distinct. It can be seen that the diagonal smaller petals (blue) are reintroduced similar to the case for $\phi = 0.3t_0$ with $\omega = 0$ [Fig. 3(b)]. In other words, the increasing ϕ can be partly compensated by going to negative bias voltage. This introduces new intra- and intersheet scattering processes connected with the smaller (blue) petals and labeled by $\tilde{\mathbf{q}}_1^a$, $\tilde{\mathbf{q}}_2^{a,b}$ in addition to the $\mathbf{q}_i^\alpha$ already defined before [Fig. 5(a)]. In general, the intrapetal scattering is still very clearly visible in the integrated QPI spectra leading to the center ellipsoids. The axis oriented ellipsoids are always present and their size depends on ω, i.e., on the size of the larger (red) petals. On the other hand, the diagonal ellipsoids in QPI spectrum are only there for negative bias voltage because they originate from the smaller (blue) petals as the characteristic wave vectors $\tilde{\mathbf{q}}_1^a$ clearly indicate. The Γ-centered ellipsoids lead to envelopes that appear as two nested squares with diagonal (large) and axis (small) orientation [Fig. 7 for $\omega = 0$].

Furthermore, the diagonal corner lobes are associated with intersheet scattering ($\mathbf{q}_3^{b-d}$-type) between the large (red) petals. Generally, intersheet scattering features are diminished and distorted due to the k_z summation. In fact, for $\omega/t_0 = 0.124$, the diagonal corner lobes have become invisible and only a remnant of the axis-aligned $\mathbf{q}_2^a$-type interpocket scattering remains. On the other hand, for $\omega/t_0 = -0.124$, the $\tilde{\mathbf{q}}_2^{a,b}$-type intersheet scattering from the small (blue) petals is visible in the QPI as new axis aligned lobes. They are, however, superposed to the weak $\mathbf{q}_2^a$-type scattering between the larger

petals. Most importantly, Fig. 7 (second row) demonstrates that clear but subtle evidence for the C_4 symmetry breaking remains in the total QPI for E_-. For $\omega = 0, -0.124t_0$, clearly, the corner lobes from inter-pocket $\mathbf{q}_3^{b-d}$-type scattering break the C_4 symmetry. For $\omega = 0.124t_0$, these are no longer visible but the center lobes now have different width for those oriented along k_x,k_y directions. On the other hand, the total A_{2+} QPI spectrum keeps full C_4 symmetry for all frequencies.

In the experimental QPI spectrum [11], the two nested square envelopes of the Γ-centered ellipsoids from intrapetal scattering are clearly visible where their relative intensity changes with frequency (voltage). For the lower frequencies, the axis and diagonal oriented lobes at larger wave vectors due to interpetal scattering are also present. However, there seems to be no easily recognizable rotational symmetry breaking present. As mentioned, the latter may only appear in single domain samples of E_- type HO.

Finally, we discuss the influence of the proposed chiral superconducting order within HO state on the QPI spectrum. In Fig. 8(a), the spectral function in HO phase (dashed red line) is superposed to the SC gap contour plot in k_x-k_z plane. Clearly, the node line $k_z = 0$ crosses the FS sheet while the node points miss it. This means in the SC phase we obtain an effectively 2D slice around $k_z = 0$ for the spectral function (blue full line). The embedding of SC into the HO phase is demonstrated by the two superposed gaps in the DOS of Fig. 8(b). For QPI, we assume the case $\omega < \Delta_0 \ll \Delta_{\mathrm{HO}}$. Due to the $k_z = 0$, a node line of the SC gap opens up only for $|k_z| > 0$ slices and strongly reduces their contribution to the total QPI. Then the latter becomes *effectively 2D* in the SC phase despite the 3D Fermi surface. Therefore the chiral d-wave SC state should be favorable to unveil the QPI structures of the HO phase with more clarity as demonstrated by the comparison of Figs. 8(c) and 8(d). Indeed, the full QPI of Fig. 8(d) in the SC + HO state is practically identical to the partial QPI of $k_z = 0$ slice in the HO phase [Fig. 5(b)] without SC gap. This is obvious from the quasi-2D shape of the (blue) spectral function in Fig. 8(a). Although the $k_z = 0$ node line of the gap is favorable for enhancing the QPI features due to HO, there is a drawback: because $|k_z| > 0$ contributions will be suppressed, the C_4 symmetry breaking in the E_- phase, which they cause, will also be suppressed. Therefore, in the HO + SC

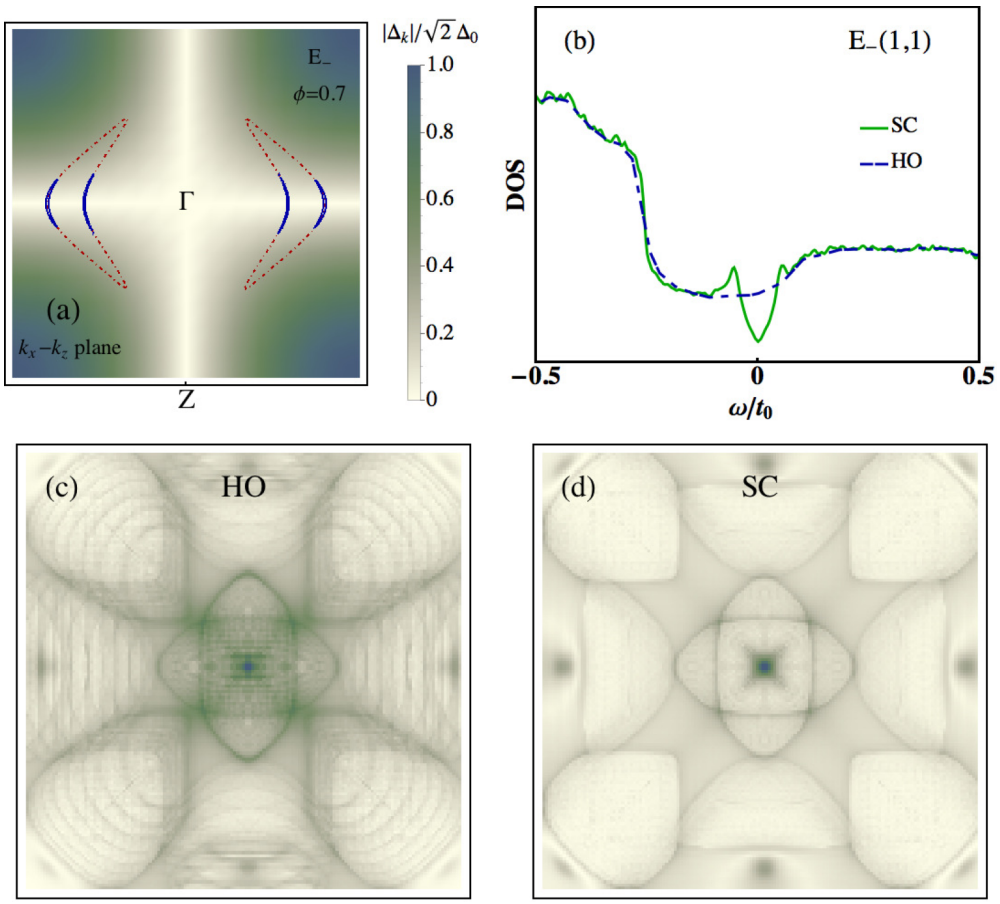

FIG. 8. (Color online) (a) Size of the gap function [Eq. (35)] on the HO Fermi surface in k_x-k_z plane. The dashed red curves show the spectral function at energy $\omega = 0$ for hidden ordered phase and blue thick curves show the quasi-2D spectral function at energy $\omega = 0.3\Delta_0$ in HO + SC phase. Note that the node line $\Delta_{\mathbf{k}} = 0$ is in $k_z = 0$ plane. (b) The DOS shows the evolution of the SC pseudogap on top of the larger HO gap. Comparison of total QPI (absolute value) image of (c) E_- HO phase ($\phi = 0.7$) [equivalent to Fig. 7(d)] with (d) HO (E_- or A_{2+}) + chiral d-wave SC phase ($\phi = 0.7, \Delta_0 = 0.1$). In the HO phase (c), the k_z summation leads to the appearance of C_4 symmetry breaking. In the HO + SC phase, the gapping of states with $|k_z| > 0$ in (a) reduces (d) to a quasi-2D QPI spectrum that contains only the C_4 symmetric $k_z = 0$ slice and therefore is equivalent for E_- or A_{2+} HO. The momentum range is given by $-\pi \leqslant k_i \leqslant \pi$.

phase, the QPI pattern of E_- and A_{2+} will be indistinguishable for $\omega < \Delta_0 \ll \Delta_{\rm HO}$.

VIII. SUMMARY AND CONCLUSION

In this work, we have performed an analysis of the consequences and signature of hidden order and chiral d-wave superconductivity in the STM quasiparticle interference of URu_2Si_2. This work was motivated on one hand by already existing experiments and on the other hand by the continuing debate on the proper symmetry of the hidden order. Our calculations are based on a simplified effective model of Ref. [12] that reproduces the main nesting Fermi surface sheets of URu_2Si_2 thought to be responsible for the multipolar HO. In particular, we studied the two most frequently discussed order parameter symmetries, the A_{2+} (rank 4) hexadecapole and E_- (rank 5) dotriacontapole. Existing experimental evidence (Sec. III) favors the latter. Their main difference is the presence of C_4 fourfold to twofold symmetry breaking in the latter, which is absent in the former. These order parameters may be described by electron-hole pairing with nesting momentum $\mathbf{Q}$ in different total angular momentum states.

The calculation of quasiparticle bands clearly shows the breakup of large electron hole pockets of the disordered phase into smaller pockets (petals) in the HO state. While the reconstructed Fermi surface sheets are equivalent in the tetragonal plane for both symmetries, they strongly differ away from it ($|k_z| > 0$) through the presence or absence of fourfold symmetry. The symmetry breaking for E_- is directly related to the presence of interorbital hopping terms. In both HO cases, a deep gap in the DOS evolves in accordance with experimental observation.

The quasiparticle interference spectrum was calculated in the Born approximation using the four reconstructed bands. Due to the pronounced 3D character of the Fermi surface in disordered as well as HO phases, the QPI calculations have to be performed for 2D slices of constant k_z followed by a summation. The result shows that the main features of the FS reconstruction by HO can still be seen in the total QPI spectrum at various bias voltages. The most prominent features result from intrasheet scattering while the structures due to interpetal scattering are more diffuse and depend on the bias voltage size. The presence of the QPI center ellipsoids and corner or edge lobe structures and partly its frequency dependence are qualitatively similar to the experimental results [11]. The center ellipsoids may also be interpreted as nested axis- and diagonal-oriented squares.

The calculation has also shown that there are subtle distinctions between the HO symmetries, in particular the clear fourfold symmetry breaking of QPI pattern in the E_- phase in contrast to A_{2+} (Fig. 7). This is, however, observable only for scanning a single domain of the E_- phase. Averaging over domains would restore the fourfold symmetry also in the E_- HO phase. This seems to be the case in the presently existing experiments [11]. The importance of having single domain samples for observing the fourfold symmetry breaking was already emphasized in torque experiments [19] and their theoretical interpretation [14]. If single domain samples can be realized in these QPI experiments, they can give additional evidence for the HO symmetry.

The influence of the frequently discussed chiral d-wave SC order embedded in the HO phase has been investigated. Due to its node line in the basal plane, this order parameter effectively leads to a reduction of total 3D QPI to an essentially 2D spectrum with improved contrast but at the same time it suppresses any symmetry distinction between E_- and A_{2+} hidden order.

APPENDIX: KINETIC ENERGY COEFFICIENTS AND PARA PHASE BAND STRUCTURE

Here, we describe the effective $5f$ two-band model for URu_2Si_2 that is adopted from Ref. [12]. The kinetic terms in Eq. (2) are defined by the intraorbital energies ($\alpha = 1,2$ is the orbital or band index):

$$\begin{aligned} A_{\alpha\mathbf{k}} &= A^z_{\alpha\mathbf{k}} + A^\perp_{\alpha\mathbf{k}} + \frac{1}{2}\mathrm{sign}(\alpha)\Delta_{12}, \\ A^z_{\alpha\mathbf{k}} &= 8t_\alpha \cos\frac{a}{2}k_x \cos\frac{a}{2}k_y \cos\frac{c}{2}k_z, \\ A^\perp_{\alpha\mathbf{k}} &= 2t'_\alpha(\cos ak_x + \cos ak_y) + 4t''_\alpha \cos ak_x \cos ak_y - \epsilon_0, \end{aligned} \tag{A1}$$

and interorbital hopping energy

$$\begin{aligned} D_\mathbf{k} &= D'_\mathbf{k} + iD''_\mathbf{k} \\ &= t_{12}\Big[\sin\frac{a}{2}(k_x+k_y) - \mathrm{i}\sin\frac{a}{2}(k_x-k_y)\Big]\sin\frac{c}{2}k_z, \\ D'_\mathbf{k} &= 4t_{12}\sin\frac{a}{2}(k_x+k_y)\sin\frac{c}{2}k_z, \\ D''_\mathbf{k} &= -4t_{12}\sin\frac{a}{2}(k_x-k_y)\sin\frac{c}{2}k_z. \end{aligned} \tag{A2}$$

To reproduce a realistic Fermi surface model with nesting electron- and holelike pockets around the Γ and Z points of the bcc Brillouin zone, we use the following parameters [12]. The orbital energy splitting is $\Delta_{12} = 3.5$ or $\Delta \equiv 0.5\Delta_{12} = 1.75$. The nearest-neighbor hopping is $t_1 = t_2 \equiv t = -0.3$, this means orbital-independent $A^z_{\alpha\mathbf{k}} = A^z_\mathbf{k}$. Furthermore, hopping elements to next- and second-nearest neighbors are given by $t'_1 = -0.87$, $t'_2 = 0.0, t''_1 = 0.375, t''_2 = 0.25$, respectively, and the average orbital energy is $-\epsilon_0 = 0.5$. The interorbital hopping is taken as $|t_{12}| = 0.7$. All energies are given here in terms of the unit t_0. Since the total effective bandwidth [Fig. 2(a)] is $W_{\rm qp} \simeq 12t_0$ and $W_{\rm qp} = 80$ meV from tunneling results [31] this means $t_0 = 6.66$ meV.

For the computation of quasiparticle bands in the HO phase, it is also useful to introduce the following (anti-) symmetrized quantities:

$$\begin{aligned} A^\perp_\mathbf{k} &= \frac{1}{2}(A^\perp_{1\mathbf{k}} + A^\perp_{2\mathbf{k}}) \\ &= 2t'(\cos ak_x + \cos ak_y) + 4t'' \cos ak_x \cos ak_y - \epsilon_0, \\ \Delta^\perp_\mathbf{k} &= \Delta + \frac{1}{2}(A^\perp_{1\mathbf{k}} - A^\perp_{2\mathbf{k}}) \\ &= \Delta + 2\delta'(\cos ak_x + \cos ak_y) + 4\delta'' \cos ak_x \cos ak_y. \end{aligned} \tag{A3}$$

Here we defined $t' = \frac{1}{2}(t'_1 + t'_2)$, $t'' = \frac{1}{2}(t''_1 + t''_2)$ and $\delta' = \frac{1}{2}(t'_1 - t'_2)$, $\delta'' = \frac{1}{2}(t''_1 - t''_2)$.

The auxiliary functions above have the following symmetry under translation by the ordering vector $\mathbf{Q}$: $A^{\perp}_{\alpha\mathbf{k}+\mathbf{Q}} = A^{\perp}_{\alpha\mathbf{k}}$ implying also $A^{\perp}_{\mathbf{k}+\mathbf{Q}} = A^{\perp}_{\mathbf{k}}$ and $\Delta^{\perp}_{\mathbf{k}+\mathbf{Q}} = \Delta^{\perp}_{\mathbf{k}}$. On the other hand, $A^{z}_{\alpha\mathbf{k}+\mathbf{Q}} = -A^{z}_{\alpha\mathbf{k}}$ and $D_{\mathbf{k}+\mathbf{Q}} = -D_{\mathbf{k}}$.

Finally, we give the relations of the $A_{1\mathbf{k}}$, $A_{2\mathbf{k}}$ to the symmetrized coefficients $A^{\perp}_{\mathbf{k}}$, $\Delta^{\perp}_{\mathbf{k}}$ introducing $\tau = \pm$ as the new band index connected with the downfolding of the paramagnetic bct to the st BZ of the HO phase and the associated symmetry $A^{z}_{\mathbf{k}+\mathbf{Q}} = -A^{z}_{\mathbf{k}}$. We obtain

$$A^{\mathbf{k}}_{\tau+} = \tau A^{z}_{\mathbf{k}} + A^{\perp}_{\mathbf{k}} + \Delta^{\perp}_{\mathbf{k}} = \begin{Bmatrix} A_{1\mathbf{k}} & \tau = + \\ A_{1\mathbf{k}+\mathbf{Q}} & \tau = - \end{Bmatrix},$$
$$A^{\mathbf{k}}_{\tau-} = \tau A^{z}_{\mathbf{k}} + A^{\perp}_{\mathbf{k}} - \Delta^{\perp}_{\mathbf{k}} = \begin{Bmatrix} A_{2\mathbf{k}} & \tau = + \\ A_{2\mathbf{k}+\mathbf{Q}} & \tau = - \end{Bmatrix}. \tag{A4}$$

This leads to the identities

$$\tfrac{1}{2}(A_{1\mathbf{k}} + A_{2\mathbf{k}}) = A^{z}_{\mathbf{k}} + A^{\perp}_{\mathbf{k}},$$
$$\tfrac{1}{2}(A_{1\mathbf{k}} - A_{2\mathbf{k}}) = \Delta^{\perp}_{\mathbf{k}}, \tag{A5}$$

and

$$\tfrac{1}{2}(A_{1\mathbf{k}+\mathbf{Q}} + A_{2\mathbf{k}+\mathbf{Q}}) = -A^{z}_{\mathbf{k}} + A^{\perp}_{\mathbf{k}},$$
$$\tfrac{1}{2}(A_{1\mathbf{k}+\mathbf{Q}} - A_{2\mathbf{k}+\mathbf{Q}}) = \Delta^{\perp}_{\mathbf{k}}. \tag{A6}$$

The para phase ($|\boldsymbol{\phi}| = |\phi_z| = 0$) band structure is given by the first of Eq. (22). Using Eq. (A6), these four bands may also be expressed as

$$\varepsilon^{\pm}_{1}(\mathbf{k}) = \tfrac{1}{2}(A_{1\mathbf{k}} + A_{2\mathbf{k}}) \pm \sqrt{\tfrac{1}{4}(A_{1\mathbf{k}} - A_{2\mathbf{k}})^2 + |D_{\mathbf{k}}|^2},$$
$$\varepsilon^{\pm}_{2}(\mathbf{k}) = \tfrac{1}{2}(A_{1\mathbf{k}+\mathbf{Q}} + A_{2\mathbf{k}+\mathbf{Q}}) \pm \sqrt{\tfrac{1}{4}(A_{1\mathbf{k}+\mathbf{Q}} - A_{2\mathbf{k}+\mathbf{Q}})^2 + |D_{\mathbf{k}}|^2}, \tag{A7}$$

which reflects directly that the four bands are obtained by the downfolding of two bands into the st BZ of the ordered phase.

[1] J. A. Mydosh and P. M. Oppeneer, Rev. Mod. Phys. **83**, 1301 (2011).
[2] P. Santini and G. Amoretti, Phys. Rev. Lett. **73**, 1027 (1994).
[3] J.-Q. Meng, P. M. Oppeneer, J. A. Mydosh, P. S. Riseborough, K. Gofryk, J. J. Joyce, E. D. Bauer, Y. Li, and T. Durakiewicz, Phys. Rev. Lett. **111**, 127002 (2013).
[4] P. M. Oppeneer, J. Rusz, S. Elgazzar, M.-T. Suzuki, T. Durakiewicz, and J. A. Mydosh, Phys. Rev. B **82**, 205103 (2010).
[5] H. Ikeda, M.-T. Suzuki, R. Arita, T. Takimoto, T. Shibauchi, and Y. Matsuda, Nat. Phys. **8**, 528 (2012).
[6] K. Haule and G. Kotliar, Nat. Phys. **5**, 796 (2009).
[7] Y. Kasahara, T. Iwasawa, H. Shishido, T. Shibauchi, K. Behnia, Y. Haga, T. D. Matsuda, Y. Onuki, M. Sigrist, and Y. Matsuda, Phys. Rev. Lett. **99**, 116402 (2007).
[8] A. Akbari, P. Thalmeier, and I. Eremin, Phys. Rev. B **84**, 134505 (2011).
[9] M. P. Allan, F. Massee, D. K. Morr, J. V. Dyke, A. W. Rost, A. P. Mackenzie, C. Petrovic, and J. C. Davis, Nat. Phys. **9**, 468 (2013).
[10] B. B. Zhou, S. Misra, E. H. da Silva Neto, P. Aynajian, R. E. Baumbach, J. D. Thompson, E. D. Bauer, and A. Yazdani, Nat. Phys. **9**, 474 (2013).
[11] A. R. Schmidt, M. H. Hamidian, P. Wahl, F. Meier, A. V. Balatsky, J. D. Garrett, T. J. Williams, G. M. Luke, and J. C. Davis, Nature (London) **465**, 570 (2010).
[12] J. G. Rau and H.-Y. Kee, Phys. Rev. B **85**, 245112 (2012).
[13] T. Takimoto and P. Thalmeier, Phys. Rev. B **77**, 045105 (2008).
[14] P. Thalmeier and T. Takimoto, Phys. Rev. B **83**, 165110 (2011).
[15] P. Thalmeier, T. Takimoto, and H. Ikeda, Phil. Mag. **94**, 3863 (2013).
[16] T. Yuan, J. Figgins, and D. K. Morr, Phys. Rev. B **86**, 035129 (2012).
[17] T. Shibauchi, H. Ikeda, and Y. Matsuda, Phil. Mag. **94**, 3747 (2014).
[18] R. Yoshida, K. Tsubota, T. Ishiga, M. Sunagawa, J. Sonoyama, D. Aoki, J. Flouquet, T. Wakita, Y. Muraoka, and T. Yokoya, Sci. Rep. **3**, 2750 (2013).
[19] R. Okazaki, T. Shibauchi, H. J. Shi, Y. Haga, T. Matsuda, E. Yamamoto, Y. Onuki, H. Ikeda, and Y. Matsusuda, Science **331**, 439 (2011).
[20] S. Tonegawa, K. Hashimoto, K. Ikada, Y.-H. Lin, H. Shishido, Y. Haga, T. D. Matsuda, E. Yamamoto, Y. Onuki, H. Ikeda, Y. Matsuda, and T. Shibauchi, Phys. Rev. Lett. **109**, 036401 (2012).
[21] S. Tonegawa, S. Kasahara, T. Fukuda, K. Sugimoto, N. Yasuda, Y. Tsuruhara, D. Watanabe, Y. Mizukami, Y. Haga, T. D. Matsuda, E. Yamamoto, Y. Onuki, H. Ikeda, Y. Matsuda, and T. Shibauchi, Nat. Commun. **5**, 4188 (2014).
[22] S.Takagi, S. Ishihara, M. Yokoyama, and H. Amitsuka, J. Phys. Soc. Jpn. **81**, 114710 (2012).
[23] I. Kawasaki, I. Watanabe, A. Hillier, and D. Aoki, J. Phys. Soc. Jpn. **83**, 094720 (2014).
[24] H. Kusunose and H. Harima, J. Phys. Soc. Jpn. **80**, 084702 (2011).
[25] P. Fulde, *Correlated Electrons in Quantum Matter* (World Scientific, Singapore, 2012).
[26] L. Capriotti, D. J. Scalapino, and R. D. Sedgewick, Phys. Rev. B **68**, 014508 (2003).
[27] A. Akbari and P. Thalmeier, Eur. Phys. J. B **86**, 495 (2013); Europhys. Lett. **102**, 57008 (2013).
[28] H. Amitsuka, K. Matsuda, I. Kawasaki, K. Tenya, M. Yokoyama, C. Sekine, N. Tateiwa, T. C. Kobayashi, S. Kawarazaki, and H. Yoshizawa, J. Magn. Magn. Mater. **310**, 214 (2007).
[29] Y. Kasahara, H. Shishido, T. Shibauchi, Y. Haga, T. D. Matsuda, Y. Onuki, and Y. Matsuda, New J. Phys. **11**, 055061 (2009).
[30] K. Yano, T. Sakakibara, T. Tayama, M. Yokoyama, H. Amitsuka, Y. Homma, P. Miranovic, M. Ichioka, Y. Tsutsumi, and K. Machida, Phys. Rev. Lett. **100**, 017004 (2008).

[31] W. K. Park, P. H. Tobash, F. Ronning, E. D. Bauer, J. L. Sarrao, J. D. Thompson, and L. H. Greene, Phys. Rev. Lett. **108**, 246403 (2012).

[32] P. Aynajian, E. H. da Silva Neto, C. V. Parker, Y. Huang, A. Pasupathy, J. Mydosh, and A. Yazdani, Proc. Natl. Acad. Sci. USA **107**, 10383 (2010).

[33] R. Okazaki, M. Shimozawa, H. Shishido, M. Konczykowski, Y. Haga, T. D. Matsuda, E. Yamamoto, Y. Onuki, Y. Yanase, T. Shibauchi, and Y. Matsuda, J. Phys. Soc. Jpn. **79**, 084705 (2010).

[34] R. Bel, H. Jin, K. Behnia, J. Flouquet, and P. Lejay, Phys. Rev. B **70**, 220501 (2004).

[35] K. Behnia, R. Bel, Y. Kasahara, Y. Nakajima, H. Jin, H. Aubin, K. Izawa, Y. Matsuda, J. Flouquet, Y. Haga, Y. Onuki, and P. Lejay, Phys. Rev. Lett. **94**, 156405 (2005).